(2)

HDL-TR-2185

September 1990

Theoretical Temperature-Dependent Branching Ratios and Laser Thresholds of the $^5I_7 \rightarrow {}^5I_8$ Transition Levels of Ho^{3+} in Ten Garnets

by Clyde A. Morrison
Elizabeth D. Filer
Norman P. Barnes
Gregory A. Turner

U.S. Army Laboratory Command
Harry Diamond Laboratories
Adelphi, MD 20783-1197

The findings in this report are not to be construed as an official Department of the Army position unless so designated by other authorized documents.

Citation of manufacturer's or trade names does not constitute an official endorsement or approval of the use thereof.

Destroy this report when it is no longer needed. Do not return it to the originator.

UNCLASSIFIED

SECURITY CLASSIFICATION OF THIS PAGE

AD-A226 664

REPORT DOCUMENTATION PAGE

Form Approved
OMB No. 0704-0188

1a. REPORT SECURITY CLASSIFICATION Unclassified	1b. RESTRICTIVE MARKINGS
2a. SECURITY CLASSIFICATION AUTHORITY	3. DISTRIBUTION/AVAILABILITY OF REPORT Approved for public release; distribution unlimited.
2b. DECLASSIFICATION/DOWNGRADING SCHEDULE	
4. PERFORMING ORGANIZATION REPORT NUMBER(S) HDL-TR-2185	5. MONITORING ORGANIZATION REPORT NUMBER(S)
6a. NAME OF PERFORMING ORGANIZATION Harry Diamond Laboratories 6b. OFFICE SYMBOL (if applicable) SLCHD-RT-AP	7a. NAME OF MONITORING ORGANIZATION
6c. ADDRESS (City, State, and ZIP Code) 2800 Powder Mill Road Adelphi, MD 20783-1197	7b. ADDRESS (City, State, and ZIP Code)
8a. NAME OF FUNDING/SPONSORING ORGANIZATION NASA 7b. OFFICE SYMBOL (if applicable)	9. PROCUREMENT INSTRUMENT IDENTIFICATION NUMBER
8c. ADDRESS (City, State, and ZIP Code) Langley Research Center Hampton, VA 23665	10. SOURCE OF FUNDING NUMBERS PROGRAM ELEMENT NO. 611102.H4400 / PROJECT NO. AH44 / TASK NO. / WORK UNIT ACCESSION NO.

11. TITLE (Include Security Classification)
Theoretical Temperature-Dependent Branching Ratios and Laser Thresholds of the $^5I_7 \rightarrow {}^5I_8$ Levels of Ho^{3+} in Ten Garnets

12. PERSONAL AUTHOR(S)
Clyde A. Morrison (HDL), Elizabeth D. Filer and Norman P. Barnes (NASA Langley), and Gregory A. Turner (HDL)

13a. TYPE OF REPORT	13b. TIME COVERED	14. DATE OF REPORT (Year, Month, Day)	15. PAGE COUNT
Interim	FROM Apr 89 TO Apr 90	September 1990	32

16. SUPPLEMENTARY NOTATION
AMS code: 611102.H440011
HDL project: AE1051

17. COSATI CODES			18. SUBJECT TERMS (Continue on reverse if necessary and identify by block number)
FIELD	GROUP	SUB-GROUP	Branching ratios, laser threshold, rare earth, lasers, Ho^{3+}, garnets, YAG, LaLuGG, GdScAG, YScAG, GdGG, GdScGG, YGG, LuGG, LuAG, GdAG

19. ABSTRACT (Continue on reverse if necessary and identify by block number)

This report presents a comparative study of triply ionized holmium in ten garnets. The point-charge model of crystal fields is used to predict the energy levels of Ho^{3+} in YAG, LaLuGG, GdScAG, YScAG, GdGG, GdScGG, YGG, LuGG, LuAG, and GdAG. The magnetic and electric dipole transition probabilities are used to predict theoretical temperature-dependent branching ratios and laser thresholds of a quasi four-level laser for each of these garnets.

20. DISTRIBUTION/AVAILABILITY OF ABSTRACT	21. ABSTRACT SECURITY CLASSIFICATION
☒ UNCLASSIFIED/UNLIMITED ☐ SAME AS RPT. ☐ DTIC USERS	Unclassified
22a. NAME OF RESPONSIBLE INDIVIDUAL Clyde A. Morrison	22b. TELEPHONE (Include Area Code) (202) 394-2042 / 22c. OFFICE SYMBOL SLCHD-RT-AP

DD Form 1473, JUN 86 *Previous editions are obsolete.*

SECURITY CLASSIFICATION OF THIS PAGE

UNCLASSIFIED

Contents

Figures

Tables

1. Introduction

In the search for longer wavelength solid-state lasers (wavelengths longer than 1.5μm), holmium appears to be the most popular active atom. Kaminskii [1] lists over 25 different materials in which the holmium $^5I_7$ to $^5I_8$ transition, at about 2.0 μm, is known to lase. A review article [2], devoted to diode-pumped solid-state lasers, has many references to holmium as the active ion. Although many references are available [3–10], a comparative study of holmium laser materials is difficult because of experimental differences, especially in the optical quality of the crystal. To avoid the expense and time associated with growth of each of the candidate crystals, a theoretical method of evaluating laser materials is needed.

A quantum mechanical point-charge model has been developed which requires only x-ray data to predict both energy levels and dipole moments of lanthanide series active atoms. X-ray data are available for many more crystals than those which have experimentally reported holmium spectra. Thus many more potential laser materials can be considered. In addition, the quantum mechanical model predicts the matrix elements of both electric and magnetic dipole operators. Both electric and magnetic dipole moments must be calculated since they can be comparable for the $^5I_7$ to $^5I_8$ transitions. These matrix elements, or some similar quantity, are required to predict gain. If gain is known, laser thresholds can be predicted. The experimental determination of gains (including crystal growth, characterization, etc) requires considerably more effort.

Although many crystal types could be evaluated, this report is restricted to the garnets for several reasons. Among the reasons are the growth potential, the desirable mechanical properties [11], and the relatively strong crystal field associated with these materials. A measure of the strength of the crystal field has been discussed by Leavitt [12]; for the parameters we have obtained by fitting the experimental data, we obtain a value of this strength parameter, S, to be 551 cm^{-1} for Ho:YAG (yttrium aluminum garnet). This value is larger than all other host crystals considered by Leavitt.

There are two primary obstacles to achieving threshold in a holmium laser operating on the $^5I_7$ to $^5I_8$ transition. Since the $^5I_8$ manifold contains the ground level, the terminal laser level has a significant thermal population. If operation near room temperature is desired, a relatively large thermal population must be overcome. In addition, since the $^5I_7$ manifold has a long lifetime, the effective stimulated emission cross section tends to be low. The second obstacle to overcome is the loss in the laser resonator, including the loss associated with the output mirror. These two factors combine to provide a figure of merit with which the various garnets can be compared.

In the work reported here we use a quantum mechanical point-charge model to predict the crystal-field split-energy levels of holmium and the matrix elements of the dipole operators between all the levels in the $^5I_7$ and the $^5I_8$ manifolds. The calculations are for the A ion site with D_2 symmetry in the garnets of the form $A_3B_2C_3O_{12}$. X-ray data are used to obtain the crystal-field components, A_{nm}, and the even-n crystal-field components are used to calculate the crystal-field splittings. The A_{nm} with n odd are used to calculate the electric dipole transition probabilities. The magnetic dipole transition probabilities were also calculated and were found to be of the same order of magnitude as the electric dipole transition probabilities. Both transition probabilities were used to calculate the branching ratios of the $^5I_7$ levels to all the levels of the $^5I_8$ multiplet. Temperature effects were taken into account by assuming a Boltzmann distribution for each of the $^5I_7$ and $^5I_8$ multiplets. Dispersion effects of the index of refraction are included by the use of Sellmeier equations which best fit the experimentally measured index of refraction.

2. Method of Calculation

Because of the number of different operations, some details of the method of computation of the branching ratios are presented. To limit the amount of computation, we restrict the calculation of the crystal-field components to the point-charge model [13–15]. The self-induced and dipole contributions [16,17] are ignored. Instead, we consider these effects by using an effective charge method [18].

In the point-charge model, the crystal-field components, A_{nm}, are given by [13,19]

$$A_{nm} = -e^2 \sum_j q_j \frac{C_{nm}\left(\hat{R}_j\right)}{R_j^{n+1}} , \tag{1}$$

where

$$C_{nm}\left(\hat{R}_j\right) = \sqrt{4\pi/(2n+1)}\, Y_{nm}\left(\theta_j, \phi_j\right)$$

and q_j is the effective charge in units of the electronic charge on the ion at $\vec{R}_j$. The $Y_{nm}(\theta j, \phi j)$ are the usual spherical harmonics. The crystallographic data given in table 1, along with the detailed x-ray data given in table 2, were used to obtain the interionic distance of the nearest neighbors of the various sites. These distances are given in table 3. The theoretical crystal-field parameters, B_{nm}, for even-n values are given by

$$B_{nm} = \rho_n A_{nm} , \tag{2}$$

where the ρ_n values for all the rare-earth ions are given elsewhere [20].

Table 1. Crystallographic data for garnets $A_3B_2C_3O_{12}$ (A = Y, La, Gd, Lu; B = Al, Ga, Lu, Sc; C = Al, Ga), cubic O_h^{10} (Ia3d) 230

Ion	Site	Symm	*X*	*Y*	*Z*	q^a
A	24*c*	D_2	0	1/4	1/8	3
B	16*a*	C_{3i}	0	0	0	3
C	24*d*	S_4	0	1/4	3/8	1.8
O	96*h*	C_1	*x*	*y*	*z*	–1.7

[a] $q_C = -5 - 4q_O$

Table 2. X-ray data on garnets $A_3B_2C_3O_{12}$

A	B	C	Compound	*a* (Å)	*x*	*y*	*z*	Ref. [27]*
Y	Al1	Al2	YAG	12.000	–0.0306	0.0512	0.1500	a
La	Lu	Ga	LaLuGG	12.930	–0.02976	0.05819	0.15699	b
Gd	Sc	Al	GdScAG	12.376	–0.0318	0.0549	0.1558	c
Y	Sc	Al	YScAG1	12.280	–0.03089	0.05625	0.15625	d
Y	Sc	Al	YScAG2	12.251	–0.0274	0.0577	0.1558	e
Gd	Ga1	Ga2	GdGG	12.377	–0.0284	0.0549	0.1497	a
Gd	Sc	Ga	GdScGG	12.5684	–0.02887	0.05657	0.15378	f
Y	Ga1	Ga2	YGG	12.280	–0.0272	0.0558	0.1501	a
Lu	Ga1	Ga2	LuGG	12.188	–0.0252	0.0570	0.1506	b
Gd	Al1	Al2	GdAG	12.113	–0.03110	0.05090	0.1490	a
Lu	Al1	Al2	LuAG	11.906	–0.0290	0.05370	0.1509	a

**See reference 27 in Reference list.*

Table 3. Distance and multiplicity of nearest oxygen to metal ions in garnet compounds[a]
[distance in angstroms]

Compound	R_{A-O}				R_{B-O}		R_{C-O}	
YAG	2.3030	(×4)	2.4323	(×4)	1.9371	(×6)	1.7609	(×4)
LaLuGG	2.4529	(×4)	2.5436	(×4)	2.1988	(×6)	1.8785	(×4)
GdScAG	2.3636	(×4)	2.4759	(×4)	2.0819	(×6)	1.7752	(×4)
YScAG1	2.3382	(×4)	2.4397	(×4)	2.0743	(×6)	1.7715	(×4)
YScAG2	2.3059	(×4)	2.4094	(×4)	2.0629	(×6)	1.8059	(×4)
GdGG	2.3680	(×4)	2.4593	(×4)	2.0046	(×6)	1.8527	(×4)
GdScGG	2.3891	(×4)	2.4845	(×4)	2.0911	(×6)	1.8514	(×4)
YGG	2.3383	(×4)	2.4277	(×4)	1.9946	(×6)	1.8485	(×4)
LuGG	2.3025	(×4)	2.3927	(×4)	1.9865	(×6)	1.8520	(×4)
GdAG	2.3347	(×4)	2.4578	(×4)	1.9438	(×6)	1.7804	(×4)
LuAG	2.2760	(×4)	2.3832	(×4)	1.9388	(×6)	1.7597	(×4)

[a] *The quantities in parentheses are the number of oxygen ions at that distance.*

If, on the other hand, the experimental crystal-field parameters, B^e_{nm}, have been obtained by fitting experimental data, then equation (2) can be used to obtain experimental A^e_{nm} by

$$A^e_{nm} = B^e_{nm} / \rho_n \tag{3}$$

for each ion for which we have experimental B^e_{nm}. We assume that the A_{nm} are independent of the particular rare-earth ion. The effective charge on each ion (in units of the electronic charge) was taken as $q_A = 3$, $q_B = 3$, and $q_C = -5 - 4q_O$,with the oxygen charge, q_O, to be determined. This approximation can be thought of as taking the (CO_4) complex in $A_3B_2(CO_4)_3$ as being covalent with the total charge on the complex fixed at –5 (notice that this gives the valance charge of $q_C = 3$ if $q_O = -2$). The choice that only the CO_4 complex is covalent was guided by the fact that the distance between the oxygen ions and the aluminum (gallium) ions is considerably smaller ($R_{C-O} \cong 1.8$ Å) than the other interionic distance ($R_{B-O} \cong 2.0$ Å), as shown in table 3. A more nearly complete theory should probably take this distance into account and have the effective oxygen charge q_O a function of this distance R_{C-O}, so that for large R_{C-O} the effective charge q_O approaches –2. We have data on Ho^{3+} in YAG from which we have obtained B^e_{nm} by fitting experimental data [21]. A more detailed discussion of the results on YAG is given in the following section.

3. Yttrium Aluminum Garnet (YAG)

The free-ion Hamiltonian used in the analysis is of the form

$$H_{FI} = E^1 e_1 + E^2 e_2 + E^3 e_3 + \alpha L(L+1) + \beta G(G_2) + \gamma G(R_7) + \zeta \sum_i \mathbf{l}_i \cdot \mathbf{s}_i \tag{4}$$

with the aqueous parameters (cm^{-1}) [22]

$$E^1 = 6440.60, \quad E^2 = 30.22, \quad E^3 = 624.39, \quad \alpha = 23.64,$$

$$\beta = -807.20, \quad \gamma = 1278.40, \quad \zeta = -2141.3\ .$$

The e_i are operators described in detail by Judd [26], and the operators $G(G_2)$, $G(R_7)$ are the Casimir operators for the G_2 and R_7 group, respectively. The last term in equation (4) is the spin-orbit interaction with the sum on i covering the 10 electrons of the $4f^{10}$ configuration of Ho^{3+}. The free-ion wave functions used throughout the analysis are those determined by equation (4) along with the aqueous parameters.

Since we have experimental data on the spectra of Ho^{3+} in YAG, we can check how well the procedure employing the point-charge model compares with the actual experimental data. The experimental data (135 levels, with an rms = 4.2 cm^{-1} [21]) were least-squares fitted, varying the crystal-field parameters, B_{nm},

in the crystal-field interaction:

$$H_{CEF} = \sum_{nm} B^{*}_{nm} \sum_{i=1}^{N} C_{nm}(\hat{r}_i) \ . \tag{5}$$

The B_{nm} (cm^{-1}) of equation (5), determined by least-squares fitting of the data of Gruber et al [21], are

$$\begin{array}{lll} B_{20} = 537 & B_{22} = 60.5 & B_{40} = -268 \\ B_{42} = -1557 & B_{44} = -785 & B_{60} = -1039 \\ B_{62} = -363 & B_{64} = 558 & B_{66} = -344 \ . \end{array} \tag{6}$$

There are four irreducible representations (IR), Γ_i, for ions having an even number of electrons in D_2 symmetry [27], and although the IR of each level was not determined experimentally, in fitting the data we accounted for the fact that the transition $\Gamma_i \rightarrow \Gamma_i$ is forbidden in both electric and magnetic dipoles.

The B_{nm} in equation (6) were used in equation (3) to determine a set of experimental crystal-field components A^{e}_{nm} (the B_{nm} of eq (6) are B^{e}_{nm}). The point-charge crystal-field components were then calculated using equation (1) with the constituent ions having the charge $q_Y = 3$, $q_{Al1} = 3$ and $q_{Al2} = -5 - 4q_O$. The resulting A_{nm} as a function of q_O were varied to find the best least-squares fit to the A^{e}_{nm} to give the value $q_O = -1.78$. A set of crystal-field parameters, B_{nm}, was calculated using equation (2) for $q = -1.7$ and ρ_n from Morrison and Leavitt [20]. Using these values of B_{nm}, we calculated the energy levels of Ho^{3+}: the splitting of the $^5I_8$ manifold was 756 cm^{-1} and that of the $^5I_7$ was 381 cm^{-1}. On the other hand, for the best fit parameters (eq (6)) the splitting of the $^5I_8$ was 521 cm^{-1} and the splitting of the $^5I_7$ was 256 cm^{-1}. Although the above procedure works quite well for many of the rare-earth ions, it is not sufficiently accurate for our purposes here. If more data were available on Ho^{3+} in garnet structures (we have found only Ho:YAG and Ho:YGG (yttrium gallium garnet) [1] reported), the point-charge model of crystal-field components, A_{nm}, could be augmented with the self-induced and dipole contributions [16,17].

We have therefore decided to approach the problem of finding the theoretical B_{nm} in a different way. To obtain better theoretical B_{nm} for Ho^{3+} in garnets, we introduce the concept of rotational invariance [12], $S_n(X)$, defined here by

$$S_n(X) = \left[\sum_{m=-n}^{n} X^{*}_{nm} X_{nm} \right]^{1/2} , \tag{7}$$

where the X_{nm} are spherical tensors such as A_{nm}, B_{nm}, etc. The values of ρ_n are calculated using equation (1) for A_{nm} with $q_O = -1.7$ and the relation,

$$\rho_n = S_n(B) / S_n(A) \ , \tag{8}$$

with the best fit B_{nm} of equation (6) to obtain

$$\rho_2 = 0.09411 \text{ Å}^2 ,$$
$$\rho_4 = 0.2922 \text{ Å}^4 , \quad (9)$$
$$\rho_6 = 0.6854 \text{ Å}^6 .$$

With these values of ρ_n, and A_{nm} values for $q_Q = -1.7$, we obtain the set of crystal-field parameters given in table 4 for Ho^{3+} in all the garnets considered.

The energy levels of Ho^{3+} were calculated with the B_{nm} given in table 4. The levels of the $^5I_8$ and $^5I_7$ multiplets are given in table 5 along with the energy levels calculated using the best-fit B_{nm} for Ho:YAG. The first column in table 5 gives the number of the energy level which will be used later when referring to a particular transition. That is, the transition from the lowest level of the $^5I_7$ multiplet to the ground state will be referred to as $18 \rightarrow 1$.

As a check on the theoretical B_{nm} predictions found by using the radial factors from the YAG data, we compared experimental and theoretical energy levels for YGG. YGG was the only other host besides YAG that had experimental energies available from the literature. An rms deviation of less than 17 cm^{-1} was obtained for the two manifolds, for 28 levels between 0 and 5391 cm^{-1}. Based on the above results, the set of theoretical B_{nm} given in table 4 for the other garnets should give good estimates of the energy levels.

With $q_Q = -1.7$, the odd-n A_{nm} are obtained with equation (5) and are listed in table 6. The odd-n A_{nm} were used in the calculation of the electric dipole transition probabilities. The method of calculating the transition probabilities is that of Judd and Ofelt [23,24]. The details of this calculation have been presented by Leavitt and Morrison [25]. The intensity calculation gives the line-to-line matrix elements of both electric dipole and magnetic dipole operators; these results were used to calculate the branching ratios of the 15 levels of the $^5I_7$ multiplet to the 17 levels of the $^5I_8$ multiplet. Since for this particular case, the magnetic dipole matrix elements are almost as large as the

Table 4. Theoretical crystal-field parameters, B_{nm} (cm^{-1}), for Ho^{3+} in 24c site (D_2 symmetry) for garnets listed in table 2

B_{nm}	1 YAG	2 LaLuGG	3 GdScAG	4 YScAG1	5 YScAG2	6 GdGG	7 GdScGG	8 YGG	9 LuGG	10 GdAG	11 LuAG
B_{20}	409	343	529	483	347	110	264	72.2	10.4	350	305
B_{22}	233	126	254	210	7.06	93.9	97.6	23.4	-104	260	160
B_{40}	-67.2	-5.46	25.6	11.4	-85.0	-72.8	-40.6	-99.9	-153	-56.1	-73.3
B_{42}	-1573	-1256	-1456	-1562	-1689	-1440	-1406	-1545	-1680	-1467	-1728
B_{44}	-787	-590	-660	-719	-812	-771	-697	-833	-914	-749	-878
B_{60}	-1101	-672	-888	-951	-1019	-913	-829	-982	-1064	-1019	-1190
B_{62}	-427	-326	-421	-454	-478	-334	-357	-363	-400	-377	-467
B_{64}	428	336	389	441	514	422	400	476	550	390	517
B_{66}	-378	-279	-347	-380	-386	-340	-322	-363	-382	-355	-430

Table 5. Energy levels (cm^{-1}) of $^5I_8$ and $^5I_7$ multiplets of Ho^{3+} based on theoretically determined B_{nm}

No.	YAG[a]		YAG[b]		LaLuGG		GdScAG		YScAG1		YScAG2		GdGG		GdScGG		YGG		LuGG		GdAG		LuAG	
	IR	E	IR	E	IR	E	IR	E	IR	E	IR	E	IR	E	IR	E	IR	E	IR	E	IR	E	IR	E
1	2	0	2	0	2	0	2	0	2	0	2	0	2	0	2	0	2	0	2	0	2	0	2	0
2	4	2	4	3	4	2	4	3	4	4	4	3	4	3	4	2	4	3	4	3	4	3	4	4
3	1	40	1	32	1	5	1	12	1	12	1	15	1	23	1	15	1	26	1	29	1	30	1	31
4	3	44	3	44	3	9	3	20	3	20	3	22	3	33	3	21	3	35	3	36	3	43	3	44
5	2	142	4	116	2	76	2	105	2	104	2	110	4	70	2	81	2	75	2	83	4	96	2	110
6	1	147	2	119	3	81	3	112	3	112	3	121	2	71	1	87	1	76	1	85	1	103	4	115
7	3	152	1	120	1	85	4	115	4	119	1	125	1	71	4	89	4	79	4	93	2	104	1	117
8	4	154	3	129	4	86	1	117	1	120	4	131	3	80	3	89	3	86	3	96	3	112	3	123
9	2	395	2	393	2	287	2	353	2	377	2	406	2	336	2	328	2	364	2	400	2	361	2	427
10	4	418	4	411	4	299	4	360	4	389	4	432	4	360	4	347	4	391	4	430	4	377	4	451
11	1	452	1	432	1	309	1	377	1	406	1	447	1	370	1	358	1	401	1	440	1	396	1	470
12	3	458	3	467	3	334	3	404	3	438	3	477	3	398	3	387	3	426	3	459	3	430	3	510
13	1	492	1	480	1	337	1	413	1	449	2	485	4	403	4	396	4	433	2	462	1	441	2	525
14	3	501	4	496	4	348	4	448	2	474	1	490	2	411	1	397	2	434	4	473	4	456	4	531
15	4	503	2	499	3	348	3	449	4	474	4	493	1	417	2	403	1	445	1	483	2	464	1	531
16	2	520	3	505	2	360	2	453	3	476	3	504	3	427	3	405	3	466	3	517	3	466	1	538
17	1	522	1	506	1	366	1	457	1	480	1	509	1	428	1	414	1	466	1	519	1	471	3	546
18	4	5227	2	5224	2	5154	2	5190	2	5202	4	5215	4	5186	4	5179	4	5196	4	5208	2	5206	2	5238
19	2	5230	4	5228	4	5155	4	5192	4	5204	2	5218	2	5186	2	5179	3	5197	3	5210	4	5212	4	5240
20	3	5238	3	5237	3	5169	3	5213	3	5222	3	5227	3	5187	3	5188	2	5200	2	5219	3	5219	3	5246
21	1	5248	1	5246	1	5176	1	5218	1	5231	1	5245	1	5206	1	5200	1	5221	1	5240	1	5227	1	5265
22	3	5302	3	5268	3	5201	3	5241	3	5257	3	5287	3	5228	3	5226	3	5249	2	5272	3	5243	3	5289
23	4	5313	2	5287	2	5210	2	5252	2	5269	4	5296	2	5238	2	5236	2	5254	3	5279	2	5261	2	5308
24	2	5320	4	5289	4	5212	4	5259	4	5273	2	5297	4	5245	4	5240	4	5266	1	5284	4	5265	4	5310
25	1	5338	1	5326	1	5237	1	5297	1	5310	1	5318	1	5256	1	5260	1	5269	4	5295	1	5299	1	5339
26	2	5351	2	5350	2	5257	2	5320	2	5332	2	5341	2	5290	2	5285	2	5309	2	5338	2	5327	2	5365
27	1	5379	1	5371	1	5285	3	5338	1	5357	1	5384	1	5325	1	5319	1	5350	1	5384	1	5345	1	5396
28	4	5394	3	5375	3	5290	4	5338	3	5360	3	5401	3	5335	3	5328	3	5363	3	5403	3	5347	3	5407
29	3	5399	4	5384	4	5292	1	5340	4	5363	4	5403	4	5350	4	5334	4	5377	4	5408	4	5357	4	5419
30	2	5415	2	5397	2	5303	2	5353	2	5378	2	5421	2	5360	2	5346	2	5390	3	5418	2	5368	2	5433
31	3	5481	3	5479	3	5357	3	5445	3	5458	3	5454	3	5390	3	5389	3	5404	4	5431	3	5451	3	5493
32	4	5483	4	5481	4	5358	4	5446	4	5459	4	5457	4	5392	4	5390	4	5407	2	5433	4	5452	4	5494

[a] *Best fit B_{nm} of equation (5).*
[b] *B_{nm} from table 4.*

Table 6. Odd-n crystal-field components, A_{nm} ($cm^{-1}/Å^n$), for 24c site (D_2 symmetry) of garnets listed in table 2[a]

A_{nm}	YAG	LaLuGG	GdScAG	YScAG1	YScAG2	GdGG
A_{32}	-1252	1539	945	1323	1315	-598
A_{52}	-2311	-1549	-1969	-2084	-2203	-1915
A_{54}	1271	889	1103	1180	1247	1112
A_{72}	31.8	61.6	47.4	67.5	96.5	66.7
A_{74}	245	88.6	140	144	178	187
A_{76}	-200	-137	-169	-191	-226	-180

A_{nm}	GdScGG	YGG	LuGG	GdAG	LuAG
A_{32}	636	-448	-262	-1412	-614
A_{52}	-1819	-2045	-2202	-2137	-2451
A_{54}	1040	1194	1293	1181	1386
A_{72}	67.5	83.8	110	28.1	68.0
A_{74}	143	206	235	222	253
A_{76}	-169	-204	-238	-180	-235

[a]*Note: All A_{nm} values are imaginary.*

electric dipole matrix elements, we are forced to use both in the branching ratio calculation. In the calculation of the branching ratios, we used the relation for the radiative lifetime given by

$$\frac{1}{\tau_{ij}} = \frac{32\pi^3\alpha}{3c^2}\left(X_{ij}\,S_{ij}^{ed} + X_{ij}^{'}\,S_{ij}^{md}\right)\nu_{ij}^3 \ , \tag{10}$$

where

$$X_{ij} = \frac{n_{ij}\left(n_{ij}^2+2\right)^2}{9} \ , \tag{11}$$

$$X_{ij}^{'} = n_{ij}^3 \ , \tag{12}$$

n_{ij} is the index of refraction at the wavelength $\lambda_{ij}\left(\lambda_{ij}\,(\mu\mathrm{m}) = \frac{10^4}{E_i - E_j}\right)$, and α is the fine structure constant.

The branching ratios as a function of temperature are given by

$$\beta_{ij}(T) = \frac{\frac{Z_i}{\tau_{ij}}}{\sum_{ij}\frac{Z_i}{\tau_{ij}}} \ , \tag{13}$$

$$Z_i = \frac{e^{-E_i/kT}}{\sum_i e^{-E_i/kT}} \ , \tag{14}$$

with the range of the sums given by

$$i = 18\text{–}32, j = 1\text{–}17 \ , \tag{15}$$

and this range will be assumed throughout. That is, i belongs to the $^5I_7$ multiplet and j belongs to the $^5I_8$ multiplet. The S_{ij}^{ed} and S_{ij}^{md} are the squared matrix elements related to the electric and magnetic dipole operators; details of their computation are given by Leavitt and Morrison [25].

To perform the calculation of the branching ratios given in equation (13), we must have the index of refraction for a large range of wavelengths. To achieve this, the experimental index of refraction is fitted to a Sellmeier equation of the form

$$n^2 = A + B\lambda^2 / (\lambda^2 - C) + D\lambda^2 / (\lambda^2 - E) \ . \tag{16}$$

For the garnets investigated here, the coefficients in the Sellmeier equations used to calculate n are given in table 7; for those garnets for which we do not have experimental data, we indicate the approximations used.

The three highest branching ratios (four for YGG) for the temperature range 50 K $\leq T \leq$ 400 K, shown in figures 1 and 2, were computed using equation (13). The branching ratio at room temperature (300 K) and 75 K is largest for LuAG, which also has the lowest thermal occupation factor for the terminal state. The results of these computations are discussed further below. The branching ratio alone is of limited value in determining the merits of practical laser systems. We therefore consider the threshold condition of a quasi-four-level laser system. Such a condition should provide a better evaluation of a given garnet laser's merit.

Table 7. Sellmeier coefficients for the index of refraction $n^2 = A + B\lambda^2/(\lambda^2 - C) + D\lambda^2/\lambda^2 - E)$. [Wavelength is in micrometers.]

Compound	A	B	C (μm^2)	D	E (μm^2)	Ref. [28]*
YAG	1	2.2779	0.01142	0	0	a
LaLuGG	1	2.3891	0.03781	0	0	b
GdScAG	1	2.510	0.01537	0	0	c
YScAG	1	2.420	0.01520	0	0	d
YScAG	1	2.4118	0.01477	0	0	e
GdGG	2.39841	1.35724	0.03027	2.37981	165.753	f
GdScGG	2.11233	1.63589	0.02620	0.99161	62.87	g
YGG	1	2.5297	0.019694	0	0	h
LuGG	1	2.2573	0.022833	0	0	i
LuAG	1	2.4822	0.009066	0	0	j
GdAG	1	2.0055	0.014559	0	0	j

*See reference 28 in Reference list .

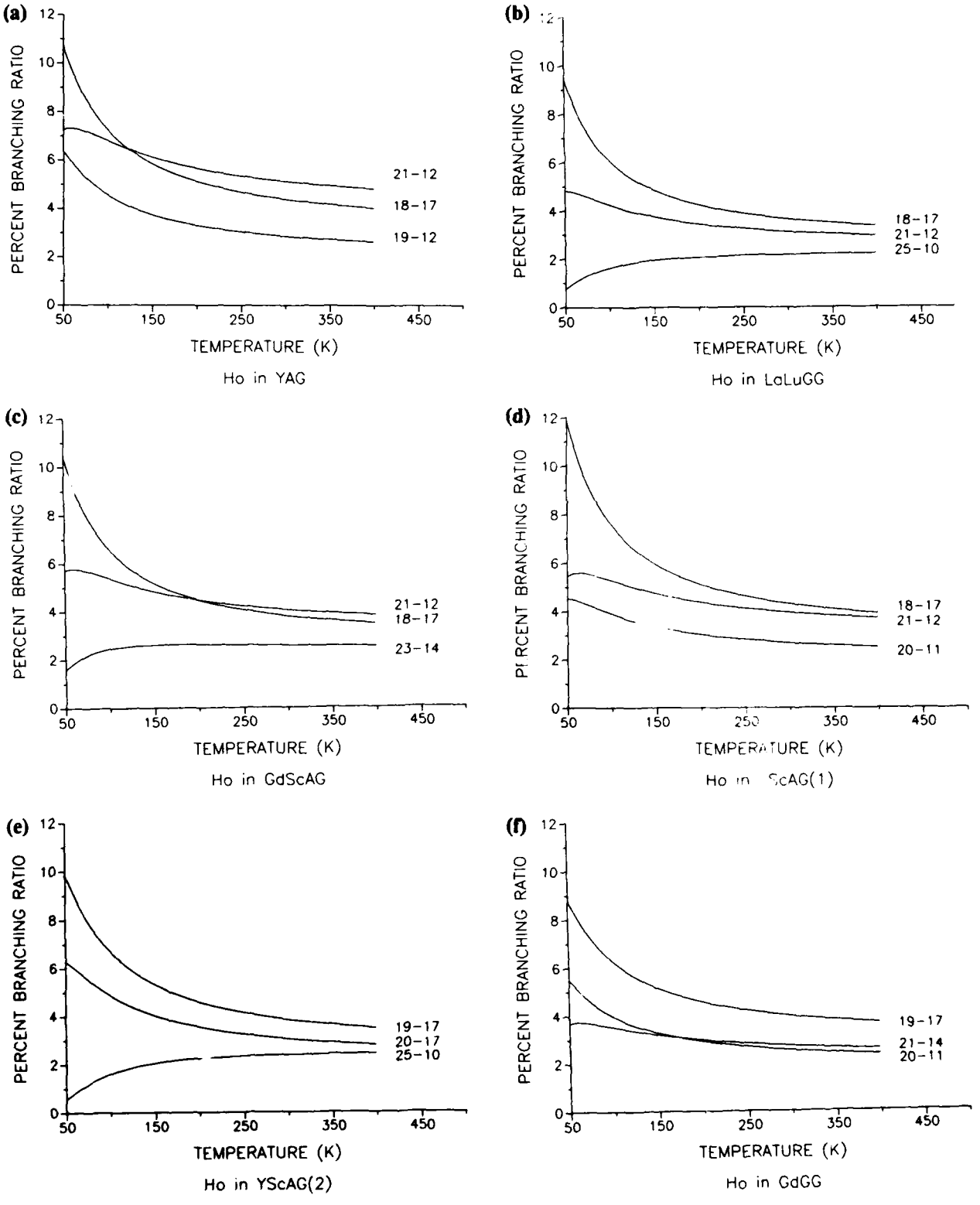

Figure 1. Branching ratio as a function of temperature for Ho^{3+} in YAG, LaLuGG, GdScAG, YScAG(1), YScAG(2), and GdGG.

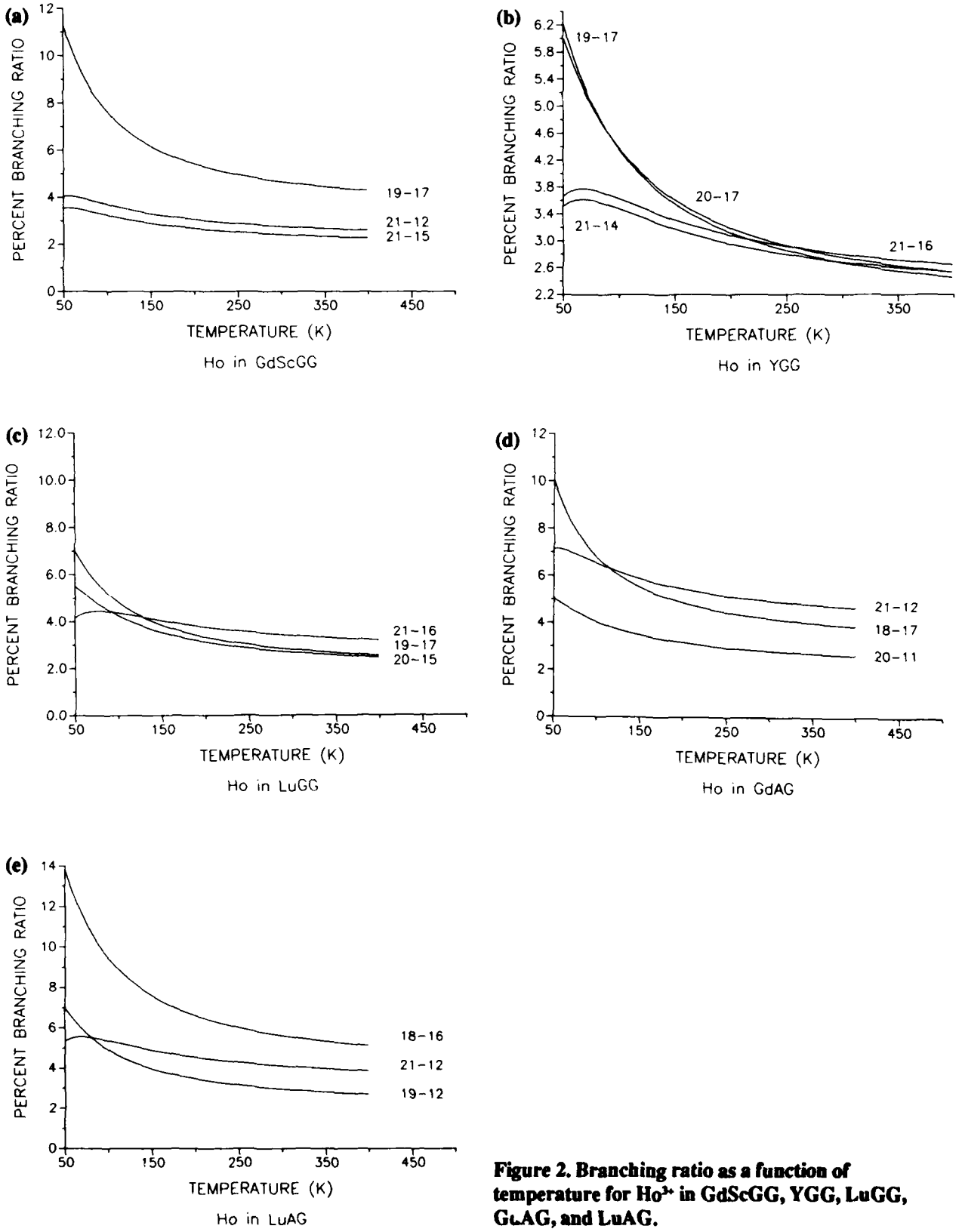

Figure 2. Branching ratio as a function of temperature for Ho^{3+} in GdScGG, YGG, LuGG, GdAG, and LuAG.

4. Threshold of Quasi-Four-Level Laser

Thresholds can be estimated with the quantities used in the calculation of branching ratios, radiative lifetimes, and energy levels. The threshold condition of a laser system can be defined as when the total loss in the laser cavity is equal to the gain of the system. For a two-level system, the threshold condition is given by [29]

$$R_m R_L \exp\left[2l\sigma_{ij}\,(N_2 Z_i - N_1 Z_j)\right] = 1 \ , \tag{17}$$

with

$$\sigma_{ij} = \lambda_{ij}^2\, g(\nu_{ij}) / (8\pi\, n_{ij}^2 \tau_{ij}) \ . \tag{18}$$

The quantity R_m is the reflectivity of the output mirror, and R_L represents the other losses in the resonator. N_2 is the density of ions in the excited state manifold ($^5I_7$), and N_1 is the density of ions in the terminal manifold ($^5I_8$). The quantity Z_i is defined in equation (14), and Z_j is a similar quantity for the terminal manifold ($^5I_8$). Throughout the discussion, the i index refers to the $^5I_7$ manifold whose number is given in the first column in table 5 ($18 \le i \le 32$), and j, to those of the $^5I_8$ multiplet ($1 \le j \le 17$). The length of the laser rod is l. It is assumed that only manifolds 1 – ($^5I_8$) and 2 – ($^5I_7$) have significant occupation; thus,

$$N_1 + N_2 = N_A \tag{19}$$

where N_A is the total number of holmium ions per unit volume.

We assume that the line shape function, $g(\nu_{ij})$, is Lorentzian with a full width at half maximum of $\Delta\nu_{ij}$ at $\nu_{ij} = \nu_o$; thus, the normalized line shape is

$$g(\nu_{ij}) = \frac{\Delta\nu_{ij}}{2\pi} \frac{1}{(\nu_{ij} - \nu_o)^2 + \left(\frac{\Delta\nu_{ij}}{2}\right)^2} \ . \tag{20}$$

Taking the logarithm of equation (17), we obtain

$$-\ln\,(R_m R_L) = 2l\sigma_{ij}\,(N_2 Z_i - N_1 Z_j) \ ; \tag{21}$$

then, using equation (19), we have

$$\frac{N_2}{N_A} = -\frac{\ln\,(R_m R_L)}{2lN_A\sigma_{ij}(Z_i + Z_j)} + \frac{Z_j}{Z_i + Z_j} \tag{22}$$

for the threshold condition for a two-level system. All the quantities on the right side of equation (22) are known, and the threshold value N_2/N_A can be computed at any temperature. This ratio can be considered a figure of merit for the particular laser system, such that the smallest N_2/N_A, in general, is the better system.

Unfortunately, for holmium, a large number of transitions lie at almost the same wavelength because of the degeneracy or near degeneracy of the energy levels of the ^5I_J multiplets. Because of the finite line widths, transitions other

than $i \rightarrow j$ can contribute significantly to the threshold. The contributions of other transitions can be taken into account by modifying equation (21) to

$$-\ln (R_m R_L) = 2l\left[\sigma_{ij} (N_2 Z_i - N_1 Z_j) + \sum_{km}{}' \sigma_{km} (N_2 Z_k - N_1 Z_m)\right] , \qquad (23)$$

where the prime on the summation indicates that $k \neq i$ and $m \neq j$ simultaneously. Using equation (19), as before, we get,

$$\frac{N_2}{N_A} = \frac{\dfrac{Z_j}{Z_i + Z_j} + G_{ij} + \sum_{km}{}' H_{ij}^{km}}{1 + \sum_{km}{}' F_{ij}^{km}} , \qquad (24)$$

where

$$G_{ij} = -\frac{\ln (R_m R_L)}{2l N_A \sigma_{ij} (Z_i + Z_j)} ,$$

$$H_{ij}^{km} = \frac{\sigma_{km} Z_m}{\sigma_{ij} (Z_i + Z_j)} ,$$

$$F_{ij}^{km} = \frac{\sigma_{km} (Z_k + Z_m)}{\sigma_{ij} (Z_i + Z_j)} .$$

In equation (24), the $i \rightarrow j$ transition is assumed to be the laser transition, so that $\nu_{ij} = \nu_o$, and we assume all line widths to be the same. With this assumption,

$$g(\nu_{ij}) = \frac{2}{\pi \Delta \nu} . \qquad (25)$$

The levels that are considered in the sum over k and m in equation (24) are determined by

$$E_k - E_m = E_i - E_j \pm \Delta E . \qquad (26)$$

In the calculation we have taken $R_m = 0.90$, $R_L = 0.90$, the laser rod length $l =$ 0.05 m, and $\Delta\nu = 3 \times 10^{11}$/s (width in energy = 10 cm^{-1}). With these assumptions, we have $n_{km} \sim n_{ij}$ and $\lambda_{km} \sim \lambda_{ij}$. Thus, in equation (24) we have

$$G_{ij} = \frac{-\ln (R_m R_L)\, 4\pi^2 \Delta\nu n_{ij}^2 \tau_{ij}}{2l N_A (Z_i + Z_j) \lambda_{ij}^2} ,$$

$$H_{ij}^{km} = \frac{\pi \Delta\nu}{2} \frac{g(\nu_{km}) \tau_{ij} Z_m}{\tau_{km} (Z_i + Z_j)} , \qquad (27)$$

$$F_{ij}^{km} = \frac{\pi \Delta\nu}{2} \frac{g(\nu_{km}) (Z_k + Z_m) \tau_{ij}}{(Z_i + Z_j) \tau_{km}} .$$

The values given in equation (27) were used in equation (24) to determine N_2/N_A for the 10 garnets considered. The lasing levels $E_i \rightarrow E_j$ were selected from the highest three values of the branching ratios calculated for each garnet. The results are shown in figures 3 and 4. The garnet with the best figure of merit (N_2/N_A, lowest at threshold) at 300 K was LuGG, while that with the best figure of merit at 75 K was YGG.

5. Results

Branching ratios were calculated for all the levels of the $^5I_7$ to $^5I_8$ manifolds for temperatures between 50 and 400 K. Plots were made for the largest lines at 300 K. YScAG was plotted twice, once for each set of x-ray data available.

The figure of merit, which is defined as the fractional population inversion required for threshold, is plotted for the same temperature range. Again, the lines with the highest branching ratios at 300 K were the lines plotted for the figure of merit. Any other lines that may have been close enough to contribute and had fairly large branching ratios were included in the figure of merit calculation of that line. Because contributing lines were considered in the figures of merit, it is not always true that the transition with the largest branching ratio has the lowest figure of merit. The figure of merit should be a better indication of where the lasing will occur, because it considers other factors, such as other contributing lines, manifold lifetimes, concentration of the holmium, and losses in the resonator.

The top branching ratio line for YAG shown in figure 1a illustrates this change of order. At 300 K, the line with the largest branching ratio is the 21–12 transition (2.092 mm). But this transition never has the lowest figure of merit for the parameters selected. The 18–17 transition (2.120 mm) has the lowest figure of merit at high temperatures (above 200 K), and the 19–12 transition (2.101 mm) has the lowest figure of merit at low temperatures (fig. 3a). This corresponds well to what we know from experiment: at 77 K the 2.098-mm line of YAG lases, and at 300 K the 2.12-mm line lases. The crossover point at 200 K has not been verified experimentally. For our theoretical results, the crossover point will change if we choose other values for R_m, R_L, l, and the holmium concentration. The default values we picked for all our calculations were 90-percent reflectivities, a rod length of 0.05 m, and a 0.3-percent concentration of the holmium.

No other lines were considered to significantly contribute to the 18–17 transition, but the 21–12 line had three other lines contributing: the 23–16, 24–16, and 24–17. The 19–12 also had lines contributing. That is, the 18–12, 20–13, and 22–17 transitions had their energy differences within 5 cm^{-1} of the energy difference for the 19–12 transition, and had large branching ratios.

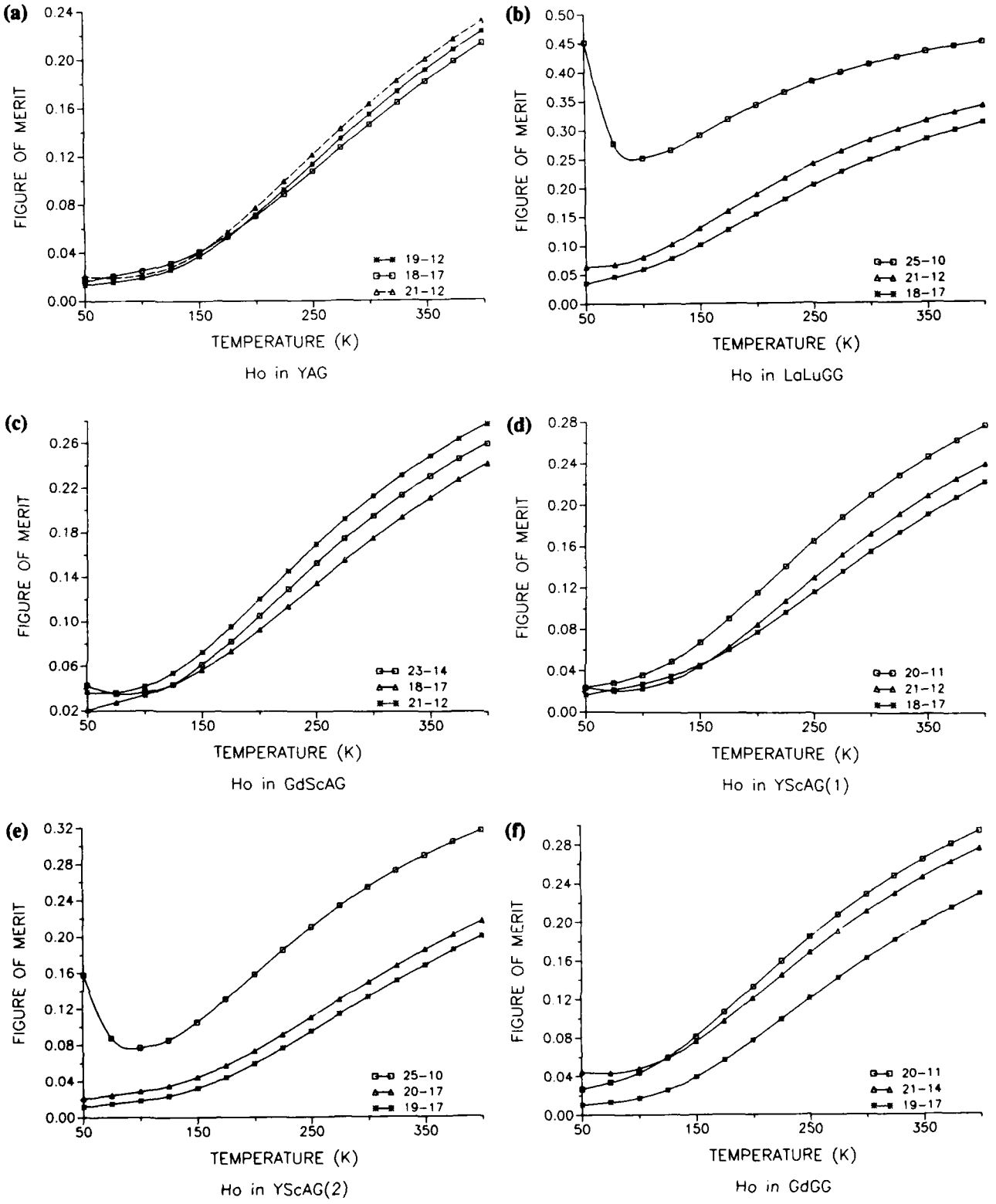

Figure 3. Figure of merit as a function of temperature for Ho^{3+} in YAG, LaLuGG, GdScAG, YScAG(1), YScAG(2), and GdGG.

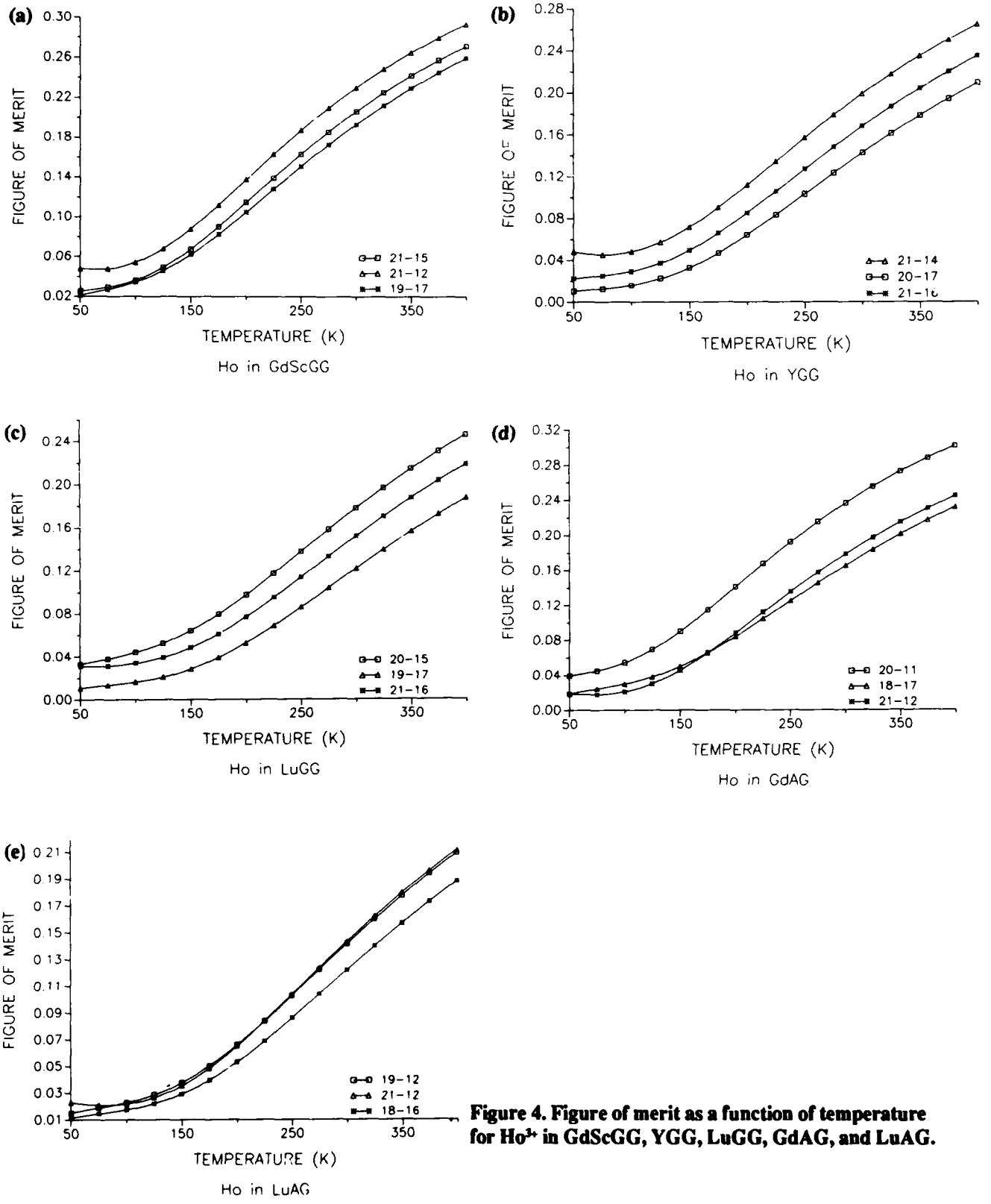

Figure 4. Figure of merit as a function of temperature for Ho^{3+} in GdScGG, YGG, LuGG, GdAG, and LuAG.

A brief discussion of the other hosts follows. For branching ratios, we looked for anything that might be unusual and for the one which was the highest. For the figure of merit, we considered which was the lowest, any crossovers that may have occurred, and any multiple lines that contributed.

LaLuGG

The highest branching ratio, at all temperatures, was the 18–17 transition (2.089 mm) (fig. 1b). In this case it was true that the highest branching ratio was also the lowest figure of merit (fig. 3b). No crossover occurred on the figure of merit. No other lines contributed to the 18–17 transition. The 21–12 line (2.067 mm) had only one other contribution, the 24–17 line. The 25–10 line (2.025 mm) had no significant contributions. One unusual discovery about this host was the large manifold lifetime. It had a value of 7023 ms, which is over 1.5 times that of YAG (3979 ms for YAG). The range of manifold lifetimes for the other hosts all fell between 3937 ms for YScAG(2) and 4750 ms for GdScGG.

GdScAG

At temperatures below 200 K, the 18–17 transition (2.113 mm) had the highest branching ratio (fig. 1c). Above this crossover point, the 21–12 line (2.078 mm) had the largest branching ratio. The 18–17 line had the lowest figure of merit at all temperatures (fig. 3c). The one exception was at 125 K, where the 23–14 line (2.082 mm) was almost as low. The 21–12 transition had only one line contributing significantly to it, the 24–15. No other lines contributed to the 18–17 transition, while three lines contributed to the 23–14 transition, namely, 20–13, 23–15, and 24–17.

YScAG(1)

The 18–17 transition had the largest branching ratio for all temperatures (fig. 1d). A double crossover occurred in the figure of merit plot (fig. 3d). Below 75 K and above 150 K, the 18–17 line (2.118 mm) was lowest. But between about 75 and 150 K, the 21–12 transition (2.087 mm) was lowest. Contributing lines were as follows: to the 18–17 line, none contributed; to the 21–12 line, 23–15, 23–16, 24–16, and 24–17 contributed; and to the 20–11 line (2.026 mm), 18–10 contributed.

YScAG(2)

The 19–17 transition had the largest branching ratio at all temperatures (fig. 1e). The 19–17 transition (2.123 mm) has the lowest figure of merit at all temperatures (fig. 3e). Contributing lines for the figure of merit calculations were as follows: for the 19–17 line, 18–17 and 19–16 contributed; for the 20–17 line (2.119 mm), again only 19–16 was close enough to contribute; for the 25–10 line (2.047 mm), 22–9 and 23–9 contributed.

GdGG

The 19–17 line (2.102 mm) had the highest branching ratio, and it was significantly higher than the next closest ones (fig. 1f). This line had by far the lowest figure of merit for this host (fig. 3f). In determining the figure of merit, we found that the 19–17 had three lines contributing: 18–17, 19–16, and 20–17. The 21–14 transition (2.085 mm) had 22–17 close enough to contribute; and the 20–11 transition (2.076 mm) had a contribution from the 18–11.

GdScGG

As in GdGG, the 19–17 (2.098 mm) transition in GdScGG also had the 19–17 (2.098 mm) transition much higher than the next closest branching ratios at all temperatures (fig. 2a). It also had the 19–17 to have the lowest figure of merit (fig. 4a). In this case, however, the 19–17 line had no contributing lines to it; the 21–12 (2.007 mm) had the 22–17 contributing; and the 21–15 (2.085 mm) had the 18–12, 19–12, and 21–16 contributing.

YGG

Above 250 K the 21–16 transition (2.103 mm) has the highest branching ratio (fig. 2b), while below this the 20–17 transition (2.703 mm) is the highest, down to 100 K. Below 100 K the 19–17 (2.114 mm) is highest. Unlike the previous two gallium garnets, the yttrium gallium garnet does not have a clear candidate for the largest branching ratio. The top several lines are close together. However, the 20–17 line does seem to have a consistent lowest figure of merit at all temperatures (fig. 4b). This may be because some strong lines such as the 19–17, 18–17 (as well as the weaker 18–16), and 20–16 are close enough to contribute to the 20–17. The 21–16 transition has only the 20–15 contributing, and the 21–14 transition (2.089 mm) has only the 22–17 contributing. Out of all the hosts, YGG had the lowest figure of merit at 75 K.

LuGG

For this host, the 21–16 (2.117 mm) had the highest branching ratio above 125 K (fig. 2c). The 19–17 (2.132 mm) was highest at lower temperatures. The line with the lowest figure of merit at all temperatures was the 19–17 (fig. 4c). The 21–16 had multiple lines (19–15 contributed), and the 19–17 had multiple lines (18–16 and 18–17 contributed), but the 20–15 (2.112 mm) did not. Compared to all other hosts, LuGG had the lowest figure of merit at 300 K.

GdAG

The highest branching ratio above about 115 K was the 21–12 transition (2.084 mm), but below this the 18–17 (2.112 μm) was higher (fig. 2d). Between 50 and 175 K the 21–12 had the lowest figure of merit; above the crossover temperature the 18–17 was lowest (fig. 4d). Multiple lines were as

follows: for the 21–12 line, the 22–13, 23–16, 24–15, 24–16, and 24–17 transitions contributed; the 18–17 had no other contributions; and the 20–11 line (2.073 mm) also had no additional contributions.

LuAG

The 18–16 (2.127 mm) was clearly the highest branching ratio, and it was much higher than the next closest (fig. 2e). This line also had the lowest figure of merit at all temperatures (fig. 4e). Multiple lines for the figure of merit were as follows: the 18–16 had no contributions; the 21–12 line (2.103 mm) had contributions from the 22–14 and the 22–16 transitions; and the 19–12 (2.114 mm) had contributions from the 18–12 line only. Out of all the other hosts, LuAG had the highest branching ratio at 75 and at 300 K, as well as the lowest thermal occupation factor for the lower laser level.

If all the hosts are compared one to another, at 300 K, LuAG had the highest branching ratio, followed by YAG, GdAG, and GdScGG. At 75 K, LuAG again had the highest branching ratio, followed by YScAG(2), GdScGG, and YAG. Additionally, LuAG had the highest energy level splitting of the lowest manifold, and was therefore found to have the lowest thermal occupation factor for the lower laser level. LuGG, YScAG(2), and YAG followed. We found that at 75 K the material with the lowest figure of merit was YGG. This was followed by GdGG, LuGG, and LuAG. But at room temperature, LuGG was found to have the best figure of merit, followed very closely by LuAG, and then by YScAG(2), and a different line of LuAG.

6. Conclusion

We evaluated 10 laser hosts by determining temperature-dependent branching ratios and figures of merit. A crystal-field model was used to predict energy levels and transition probabilities of holmium in garnet hosts. We determined a complete set of theoretical crystal-field parameters for these garnets from a set of radial factors based on experimental data available for YAG. A real need exists for more experimental energy levels for holmium in garnets. Besides YAG, YGG was the only other material that had energy levels available in the literature. Energy levels for Ho:YGG were predicted based on the theoretical crystal-field parameters, and good agreement to experiment was found. This led us to believe that our set of theoretical crystal-field parameters would give good estimates of the energy levels for the other hosts for which we had no experimental optical data. With x-ray and index of refraction data, we have evaluated the performance of 10 lasers by using a quantum mechanical model to predict the position of the energy levels and the temperature-dependent branching ratios of the $^5I_7$ to $^5I_8$ levels of holmium. The fractional population inversion required for threshold, a factor based on the branching ratios and thermal occupation factors, was also evaluated.

7. Acknowledgements

We wish to acknowledge the cooperation of John B. Gruber and Marian E. Hills for providing their detailed determination of the energy levels of Ho:YAG. Also, C. A. Morrison thanks his coworkers John Bruno and Richard Leavitt for several helpful discussions.

References

[1] A. A. Kaminskii, *Laser Crystals*, Springer-Verlag, New York (1981), chapter 5.

[2] T. Y. Fan and R. L. Byer, *Diode Laser-Pumped Solid-State Lasers*, IEEE J. Quantum Electron. **24** (1988), 895. (This review article contains 140 references.)

[3] A. N. Allat'ev, E. V. Zharikow, S. P. Katitin, V. V. Laptev, V. V. Osiko, V. G. Ostroumov, A. M. Prokhorov, Z. S. Saidov, V. A. Smirnov, I. T. Sorkokina, A. F. Umyskov, and I. A. Shcherbakov, *Lasing of Holmium Ions as a Result of the* $^5I_7 \rightarrow {}^5I_8$ *Transition at Room Temperature in a Yttrium Scandium Gallium Garnet Crystal Activated with Chromium, Thulium, and Holmium Ions*, Sov. J. Quantum Electron. **16** (1986), 1404.

[4] N. F. Barnes, D. J. Gettemy, N. J. Levinos, and J. E. Griggs, *TEM*$_{oo}$ *mode Ho:YLF Laser*, SPIE Vol. **190**, LASL Optics Conference (1979), 297.

[5] B. M. Antipenkov, A. S. Glebov, L. I. Krutova, V. M. Sointsev, and L. K. Sukhareva, *Active Medium of Lasers Operating in the 2-*μ *Spectra Range and Utilizing Gadolinium Scandium Gallium Garnet Crystals*, Sov. J. Quantum Electron. **16** (1986), 995.

[6] B. M. Antipenko, A. S. Glevob, T. I. Kizeleva, and V. A. Pis'mennyi, *2.12* μ*m Ho:YAG Laser*, Sov. Tech. Phys. Lett. **11** (1985), 284.

[7] G. Huber, E. W. Duczyndkim, and K. Petermann, *Laser Pumping of Ho-Tm-Er-doped Garnet Lasers at Room Temperature*, IEEE J. Quantum Electron. **24** (1988), 920.

[8] T. Y. Fan, G. Huber, R. L. Byer, and P. Mitzscherlich, *Spectroscopy and Diode Laser-Pumped Operation of Tm, Ho: YAG*, IEEE J. Quantum Electron. **24** (1988), 924.

[9] L. F. Johnson, J. E. Geusic, and L. G. VanUitert, *Coherent Oscillations from* Tm^{3+}, Ho^{3+}, Yb^{3+}, *and* Er^{3+} *Ions in Yttrium Aluminum Garnet*, Appl. Phys. Lett. **1** (1965), 127.

[10] G. Quarles, A. Rosenbaum, C. Marquardt, and L. Esterowitz, *High Efficiency 2.09* μ*m Flashlamp Pumped Laser*, Appl. Phys. Lett. **55** (1989), 1062.

[11] V. F. Kitaeva, E. V. Zharikov, and I. L. Chistyi, *The Properties of Crystals with Garnet Structure*, Phys. Stat. Sol. (a)**92** (1985), 475.

[12] R. P. Leavitt, *On the Role of Certain Rotational Invariants in Crystal-Field Theory*, J. Chem. Phys. **77** (1982), 1661.

[13] C. A. Morrison and R. P. Leavitt, in *Handbook on the Physics and Chemistry of Rare Earths V*, edited by K. A. Gschneidner, Jr., and L. Eyring, North Holland, NY (1982).

[14] C. A. Morrison, *Angular Momentum Theory Applied to Interactions in Solids*, Lecture Notes in Chemistry **47**, Springer-Verlag, NY (1988).

[15] C. A. Morrison, N. Karayianis, and D. E. Wortman, *Rare-Earth Ion Host Lattice Interactions: 4. Predicting Spectra and Intensities of Lanthanides in Crystals*, Harry Diamond Laboratories, HDL-TR-1816 (1977).

[16] C. A. Morrison, G. F. de Sa, and R. P. Leavitt, *Self-Induced Multipole Contribution to the Single Electron Crystal Field*, J. Chem. Phys. **76** (1982), 3899.

[17] C. A. Morrison, *Dipolar Contributions to the Crystal Fields in Ionic Solids*, Solid State Comm. **18** (1976), 153.

[18] R. P. Leavitt, C. A. Morrison, and D. E. Wortman, *Rare Earth Ion-Host Lattice Interactions: 3. Three Parameter Theory of Crystal Fields*, Harry Diamond Laboratories, HDL-TR-1673 (1975).

[19] N. Karayianis and C. A. Morrison, *Rare Earth Ion-Host Lattice Interactions: 1. Point Charge Lattice Sum in Scheelites*, Harry Diamond Laboratories, HDL-TR-1648 (1973).

[20] C. A. Morrison and R. P. Leavitt, *Crystal Field Analysis of Triply Ionized Rare Earth Ions in Lanthanum Trifluoride*, J. Chem. Phys. **71** (1979), 2366.

[21] J. B. Gruber, M. E. Hills, M. D. Seltzer, C. A. Morrison, and G. A. Turner, *Symmetry, Selection Rules, and Stark Level Assignments in* $Ho^{3+}:Y_3Al_5O_{12}$, IQEC '90, Anaheim, CA, 21–25 May 1990 (to be published).

[22] W. T. Carnall, P. R. Fields, and K. Rajnak, J. Chem. Phys. **49** (1968) 4424.

[23] B. R. Judd, *Optical Absorption Intensities of Rare-Earth Ions*, Phys. Rev. **127** (1962), 750.

[24] G. S. Ofelt, *Intensities of Crystal Spectra of Rare-Earth Ions*, J. Chem. Phys. **37** (1962), 511.

[25] R. P. Leavitt and C. A. Morrison, *Crystal Field Analysis of Triply Ionized Rare Earth Ions in Lanthanum Trifluoride–II. Intensity Calculation*, J. Chem. Phys. **73** (1980), 749.

[26] B. R. Judd, *Operator Techniques in Atomic Spectroscopy*, McGraw-Hill, New York (1963), Chapter 8.

[27] X-ray data were taken from the following:

a. C. Morrison and R. Leavitt, *Handbook on the Physics and Chemistry of Rare Earths*, K. A. Gschneidner and L. Eyring, eds., North Holland (1982), 461.
b. T. Allik, S. Stewart, D. Sardar, G. Quarles, R. Powell, C. Morrison, G. Turner, M. Kokta, W. Hovis, and A. Pinto, *Preparation, Structure, and Spectroscopic Properties of* Nd^{+3}*:* $\{La_{1-x}Lu_x\}_3[Lu_{1-y}Ga_y]_2\ Ga_3O_{12}$ *Crystals*, Phys. Rev. **B37** (1988), 9129.
c. T. Allik, private communication (7 November 1986).
d. T. Allik, C. Morrison, J. Gruber, and M. Kokta, *Crystallography, Spectroscopic Analysis, and Lasing Properties of* Nd^{3+}*:*$Y_3Sc_2Al_3O_{12}$, Phys. Rev. **B41** (1990), 21.
e. G. A. Bogomolova, L. A. Bamagina, A. A. Kaminskii, and B. Z. Malkin, Sov. Phys. Solid State **19** (1977), 1428.
f. T. Allik, private communication (9 March 1988).

[28] Ten Sellmeier coefficients were obtained from the following:

a. T. S. Lomheim and L. G. DeShazer, Phys. Rev. **B20** (1979), 4343.
b. T. Allik, S. A. Stewart, D. K. Sardar, G. J. Quarles, M. R. Kokta, W. H. Hovis, and A. A. Pinto, *Preparation, Structure, and Spectroscopic Properties of* Nd^{3+}*:* $\{La_{1-x}Lu_x\}_3\ [Lu_{1-y}Ga_y]_2\ Ga_3O_{12}$ *Crystals*, Phys. Rev. **B3** (1988), 9129.
c. T. Y. Fan et al [8], p 308 (see above).
d. T. Allik, C. A. Morrison, J. B. Gruber, and M. R. Kokta, *Crystallography, Spectroscopic Analysis, and Lasing Properties of* Nd^{3+}*:*$Y_3Sc_2Al_3O_{12}$, Phys. Rev. **B41** (1990), 21.
e. S. H. Wemple and W. J. Tabor, *Refractive Index Behavior of Garnets*, J. Appl. Phys. **44** (1973), 1395.
f. *C. R. C. Handbook of Laser Science and Technology, Vol. 5, optical materials*, part 3, 307.
g. Johnston and Dodge, J. Opt. Soc. Am. **68**.
h. T. Y. Fan et al [8], p 304 (see above).
i. Interpolated from GdGG and YGG.
j. Interpolated from YAG, GdGG, and YGG.

[29] O. Svelto and D. C. Hanna, *Principles of Lasers*, Plenum Press, New York (1982).

[30] N. P. Barnes and D. J. Gettamy, *Pulsed Ho:YAG Oscillator and Amplifier*, IEEE J. Quantum Electron. **QE-17** (1981), 1303.

Distribution

Administrator
Defense Technical Information Center
Attn DTIC-DDA (2 copies)
Cameron Station, Bulding 5
Alexandria, VA 22304-6145

Director
Night Vision & Electo-Optics Laboratory
Attn Technical Library
Attn R. Buser
Attn A. Pinto
Attn J. Hebersat
Attn R. Rhode
Attn W. Tressel
Ft Belvoir, VA 22060

Director
Defense Advanced Research Projects Agency
Attn J. Friebele
1400 Wilson Blvd
Arlington, VA 22290

Director
Defense Nuclear Agency
Attn Tech Library
Washington, DC 20305

Under Secretary of Defense Res & Engineering
Attn Tech Library, 3C128
Washington, DC 20301

Office of the Deputy Chief of Staff, for Research, Development, & Acquisition
Department of the Army
Attn DAMA-ARZ-B,
I. R./ Hershner
Washington, DC 20310

Commander
US Army Armament Munitions & Chemical Command (AMCCOM)
US Army Armament Research & Development Center
Attn DRDAR-TSS, STINFO Div
Dover, NJ 07801

Commander
Atmospheric Sciences Laboratory
Attn Technical Library
White Sands Missile Range, NM 88002

Director
US Army Ballistic Research Laboratory
Attn SLCBR-DD-T (STINFO)
Aberdeen Proving Ground, MD 21005

Director
US Army Electronics Warfare Laboratory
Attn J. Charlton
Ft Monmouth, NJ 07703

Director
US Army Electronics Warfare Laboratory
Attn DELET-DD
Ft Monmouth, NJ 07703

Commanding Officer
USA Foreign Science & Technology Center
Attn DRXST-BS, Basic Science Div
Federal Office Building
Charlottesville, VA 22901

Commander
US Army Materials & Mechanics Research Center
Attn DRXMR-TL, Tech Library
Watertown, MA 02172

US Army Materiel Command
5001 Eisenhower Ave
Alexandria, VA 22333-0001

US Army Materiel Systems Analysis Activity
Attn DRXSY-MP, Library
Aberdeen Proving Ground, MD 21005

Commander
US Army Missile & Munitions Center & School
Attn ATSK-CTD-F
Redstone Arsenal, AL 35809

Commander
US Army Missile & Munitions Center & School
Attn DRDMI-TB, Redstone Sci Info Center
Redstone Arsenal, AL 35809

Commander
US Army Research Office Durham
Attn R. J. Lontz
Research Triangle Park, NC 27709

Distribution (cont'd)

Commander
US Army Research Office Durham
Attn M. Stosio
Research Triangle Park, NC 27709

Commander
US Army Research Office Durham
Attn M. Ciftan
Research Triangle Park, NC 27709

Commander
US Army Research Office Durham
Attn R. Guenther
Research Triangle Park, NC 27709

Commander
US Army Research Office Durham
Attn C. Bogosian
Research Triangle Park, NC 27709

Commander
USA Resch & Std Gp (Europe)
Attn Chief, Physics & Math Branch
FPO, New York 09510

Commander
US Army Test & Evaluation Command
Attn D. H. Sliney
Aberdeen Proving Ground, MD 21005

Commander
US Army Test & Evaluation Command
Attn Tech Library
Aberdeen Proving Ground, MD 21005

Commander
US Army Troop Support Command
Attn DRXRES-RTL, Tech Library
Natick, MA 01762

Office of Naval Research
Attn J. Murday
Arlington, VA 22211

Director
Naval Research Laboratory
Attn Code 2620, Tech Library Br
Attn G. Quarles
Attn G. Kintz
Attn A. Rosenbaum
Attn G. Risenblatt

Director
Navel Research Laboratory (cont'd)
Attn Code 5554, F. Bartoli
Attn Code 6540, Dr. S. R. Bowman
Attn Code 5554, L. Esterowitz
Attn Code 5554, R. E. Allen
Washington, DC 20375

Commander
Naval Weapons Center
Attn Code 3854, R. Schwartz
Attn Code 3854, M. Hills
Attn Code 3854, M. Nadler
Attn Code 385, R. L. Atkins
Attn DOCE 343, Technical Information Department
China Lake, CA 93555

Air Force Office of Scientific Research
Attn Major H. V. Winsor, USAF
Bolling AFB
Washington, DC 20332

HQ, USAF/SAMI
Washington, DC 20330

Department of Commerce
National Bureau of Standards
Attn Library
Washington, DC 20234

Nasa Langley Research Center
Attn N. P. Barnes (20 copies)
Attn G. Armagan
Attn P. Cross
Attn D. Getteny
Attn J. Barnes
Attn E. Filer (10 copies)
Attn C. Bair
Attn N. Bounchrishani
Hampton, VA 23665

Director
Advisory Group on Electron Devices
Attn Sectry, Working Group D
201 Varick Street
New York, NY 10013

Aerospace Corporation
Attn M. Birnbaum
Attn N. C. Chang

Distribution (cont'd)

Aerospace Corporation (cont'd)
Attn T. S. Rose
PO box 92957
Los Angeles, CA 90009

Allied
Advanced Application Dept
Attn A. Budgor
31717 La Tiemda Drive
Westlake Village, CA 91362

Allied Signal Inc
Attn Y. Band
Attn R. Morris
POB 1021R
Morristown, NJ 07960

Ames Laboratory Dow
Iowa State University
Attn K. A. Gschneidner, Jr (2 Copies)
Ames, IA 50011

Argonne National Laboratory
Attn W. T. Carnall
9700 South Cass Avenue
Argonne, IL 60439

Booz, Allen and Hamilton
W. Drozdoski4330 East West Highway
Bethesda, MD 20814

Brimrose Corp of America
Attn R. G. Rosemeier
7527 Belair Road
Baltimore, MD 21236

Draper Lab
Attn F. Hakimi, MS 53555 Tech Sq
Cambridge, MA 02139

Engineering Societies Library
Attn Acquisitions Dept
345 East 47th Street
New York, NY 10017

Fibertech Inc
Attn H. R. Verdin (3 Copies)
510-A Herdon Pkwy
Herdon, VA 22070

General Dynamics
Attn R. J. Blair
5452 Oberlin Drive
San Diego, CA 92121

Hughes Aircraft company
Attn D. Sumida
3011 Malibu Canyon Rd
Malibu, CA 90265

IBM Research Division
Almaden Research Center
Attn R. M. Macfarlane, Mail Stop K32 802(d)
650 Harry Road
San Jose, CA 95120

Director
Lawrence Radiation Laboratory
Attn M. J. Weber
H. A. Koehler
W. Krupke
Livermore, CA 94550

LTV
Attn M. Kock (WT-50)
PO Box 650003
Dallas, TX 75265

Martin Marietta
Attn F. Crowne
Attn J. Little1450
Attn T. Worchesky
1450 South Rolling Road
Baltimore, MD 21227

McDonnell Douglass Electronic Systems Company
Dept Y440, Bldg. 101, Lev. 2 Rm/Pt B54
Attn D. M. Andrauskas, MS-2066267
PO Box 516
St Louis, MO 63166

MIT Lincoln Lab
Attn B. Aull
PO Box 73
Lexington, MA 02173

Distribution (cont'd)

Department of Mechanical, Industrial, & Aerospace Engineering
Attn S. Temkin
PO Box 909
Piscataway, NJ 08854

National Oceanic & Atmospheric Adm Environmental Research Labs
Attn Library, R-51, Tech Rpts
Boulder, CA 80302

Oak Ridge National Laboratory
Attn R. G. Haire
Oak Ridge, TN 37839

W. J. Schafer Assoc
Attn J. W. Collins
321 Billerica Road
Chelmsford, MA 01824

Science Applications, International Corp
Attn T. Allik
1710 Goodridge Drive
McLean, VA 22102

Shwartz Electro-Optic, Inc.
Attn G. A. Rines
45 Winthrop Street
Concord, MA 01742

Teledyne Brown Engineering
Cummings Research Park
Attn M. L. Price, MS-44
Huntsville, AL 35807

Union Carbide Corp
Attn M. R. Kokta
50 South 32nd Street
Washougal, WA 98671

Arizona State University
Dept of Chemistry
Attn L Eyring
Tempe, AZ 85281

University of Southern California
Attn Dr. M. Birnbaum
Denney Research Bldg., University park
Los Angeles, CA 90089

Carnegie Mellon University
Schenley Park
Attn Physics & EE, J. O. Artman
Pittsburgh, PA 15213

Colorado State University
Physics Department
Attn S. Kern
Ft Collins, CO 80523

University of Connecticut
Department of Physics
Attn R. H. Bartram
Storrs, CT 06269

University of South Florida
Physics Dept
Attn R. Chang
Attn Sengupta
Tampa, FL 33620

Howard University
Physics Department
Attn Prof. V. Kushamaha
25 Bryant St., N.W.
Washington, DC 20059

Johns Hopkins University
Dept of Physics
Attn B. R. Judd
Baltimore, MD 21218

Kalamazoo College
Dept of Physics
Attn K. Rajnak
Kalamazoo, MI 49007

Massachusetts Institute of Technology
Crystal Physics Laboratory
Attn H. P. Jenssen
Attn A. Linz
Cambridge, MA 02139

Massachusetts Institute of Technology
Attn V. Bagnato
77 Mass, Ave, Room 26-251
Cambridge, MA 02139

Distribution (cont'd)

University of Minnesota, Duluth
Department of Chemistry
Attn L. C. Thompson
Duluth, MN 55812

Oklahoma State University
Dept of Physics
Attn R. C. Powell
Stillwater, OK 74078

Pennsylvania State University
Materials Research Laboratory
Attn W. B. White
University Park, PA 16802

Princeton University
Department of Chemistry
Attn D. S. McClure
Princeton, NJ 08544

San Jose State University
Department of Physics
Attn J. B. Gruber
San Jose, CA 95192

Seaton Hall University
Chemistry Department
Attn H. Brittain
South Orange, NJ 07099

University of Virginia
Dept of Chemistry
Attn F. S. Richardson (2 Copies)
Charlottesville, VA 22901

University of Wisconsin
Chemistry Department
Attn J. Wright
Attn B. Tissue
Madison, WI 53706

US Army Laboratory Command
Attn Technical Director, AMSLC-TD

Installation Support Activity
Attn Legal Office, SICIS-CC

USAISC
Attn Record Copy, AMSLC-IM-TS

USAISC (cont'd)
Attn Technical Reports Branch,
AMSLC-IM-VP (2 copies)

Harry Diamond Laboratories
Attn Division Directors
Attn Library, SLCHD-TL (3 copies)
Attn Library, SLCHD-TL (Woodbridge)
Attn Chief, SLCHD-NW-CS
Attn Chief, SLCHD-NW-E
Attn Chief, SLCHD-NW-EH
Attn Chief, SLCHD-NW-EP
Attn Chief, SLCHD-NW-ES
Attn Chief, SLCHD-NW-P
Attn Chief, SLCHD-NW-R
Attn Chief, SLCHD-NW-RP
Attn Chief, SLCHD-NW-RS
Attn Chief, SLCHD-NW-TN
Attn Chief, SLCHD-NW-TS
Attn Chief, SLCHD-PO
Attn Chief, SLCHD-ST-C
Attn Chief, SLCHD-ST-RP
Attn Chief, SLCHD-ST-RS
Attn Chief, SLCHD-TT
Attn B. Willis, SLCHD-TA-ET
Attn B. Zabludowski, SLCHD-TA-ET
Attn C. S. Kenyon, SLHD-NW-EP
Attn J. R. Miletta, SLCHD-NW-EP
Attn F. B. McLean, SLCHD-ST-MW
Attn L. Libelo, SLCHD-ST-MW
Attn A. A. Bencivenga, SLCHD-ST-SP
Attn J. Sattler, SLCHD-CS
Attn J. Nemarich, SLCHD-ST-CB
Attn B. Weber, SLCHD-ST-CB
Attn T. Bahder, SLCHD-ST-AP
Attn J. Bradshaw, SLCHD-ST-AP
Attn J. Bruno, SLCHD-ST-AP
Attn E. Harris, SLCHD-ST-AP
Attn R. Leavitt, SLCHD-ST-AP
Attn J. Pham, SLCHD-ST-AP
Attn G. Simonis, SLCHD-ST-AP

Distribution (cont'd)

Harry Diamond Laborfatories (cont'd)
Attn M. Stead, SLCHD-ST-AP
Attn J. Stellato, SLCHD-ST-AP
Attn S. Stevens, SLCHD-ST-AP
Attn R. Tober, SLCHD-ST-AP
Attn M. Tobin, SLCHD-ST-AP

Harry Diamond Laboratories (cont'd)
Attn G. Turner, SLCHD-ST-AP (10 copies)
Attn D. Wortman, SLCHD-ST-AP
Attn C. Garvin, SLCHD-ST-SS
Attn J. Goff, SLCHD-RT-RB
Attn C. Morrison, SLCHD-ST-AP (10 Copies)